

TCV tokamak neutron shielding upgrade for dual NBI operation

H. Weisen, P. Blanchard, M. Vallar, A. N. Karpushov, J. Dubray, A. Merle, B. P. Duval,
J. Cazabonne, D. Testa, H. Hamac Elaïan and the TCV team*
*Ecole Polytechnique Fédérale de Lausanne (EPFL), Swiss Plasma Center (SPC),
CH-1015 Lausanne, Switzerland*

A. Žohar, L. Snoj, B. Kos¹, M. Fortuna, A. Čufar
Jožef Stefan Institute, Jamova cesta 39, 1000 Ljubljana, Slovenia

F. Tesse, F. Fontana, C. Gloor, R. Iannarelli, H. Palacios, C. Tille,
*Ecole Polytechnique Fédérale de Lausanne (EPFL),
Development and Construction (VPO-DC)
CH-1015 Lausanne, Switzerland*

M. Molteni
Willy Ingénieurs, av. du 14-Avril 20, 1020 Renens, Switzerland

*see author list of H. Reimerdes et al 2022 Nucl. Fusion 62 042018

¹ Currently at ORNL, Oak Ridge, USA

Abstract. The Tokamak à Configuration variable (TCV) is equipped with two Neutral Beam Injection (NBI) systems delivering up to 1.2 MW each for pulse durations of up to 2 seconds. The first system (NBI1), designed for an injection energy in the range 25 keV - 30 keV has been operational since 2016. The existing concrete neutron shielding of the experimental hall proved insufficient for fully protecting human accessible areas, limiting the number of daily plasma pulses using NBI1. The recently commissioned second system (NBI2) is designed for injection synergies in the range 50 keV - 60 keV. Both systems are tangentially oriented in opposite directions in order to permit experiments with low or no net torque. Calculations with the TRANSP and ORBIS heating codes show that neutron rates from deuterium-deuterium fusion reactions may be as high as 10^{14} n/s, up to 10 times higher than with the lower energy beam only. This is due both to the ~5 times larger beam-plasma neutron rates from the higher energy beam and to an exceptionally high contribution from beam-beam reactions between the opposing beams. The radiation protection policy at SPC is that all staff members be considered as members of the general public, limiting the daily personal dose to 4 μ Sv. This is also the maximum admissible daily dose in any publicly accessible zone, whether occupied or not. Currently, with only the lower energy beam, this limit can be attained in the control room adjacent to the device hall after only 5 NBI pulses out of a possible 30 daily pulses. To allow exploitation of the two beams at full specifications, the source side of the existing barite concrete walls of the 15 m \times 20 m \times 8 m large TCV hall will be covered with 20 cm thick polythene (PE) cladding and a ceiling made of 35 cm thick polythene will be added. The total mass of PE will be 200 tons. The usage of PE at this scale for neutron shielding is unprecedented at any fusion research facility.

Keywords: radiation protection, neutron dose, tokamak, safety

I. Introduction

The scientific missions of the TCV tokamak [1] include researching plasma confinement, in particular concerning the impact of plasma shaping, the physics and control of plasma-wall interactions as well as the physics of energetic particles and energetic particle modes [2], which will dominate in future fusion reactors because of the high energy alpha particles produced by fusion reactions.

At the time of construction (1991) TCV was only intended to have Electron Cyclotron Heating (ECH) and EC current drive (ECCD) [3]. Consequently, most of the radiation exposure was expected to be from X-rays and gamma rays. The 8 m high walls of TCV experimental hall are open to the building roof (fig.1) and consist of 0.5 m thick barite concrete. This shielding proved unsatisfactory when, in 2016, the existing ECH system on TCV was complemented with a neutral beam injector (NBI1) with power 1.2 MW and 19 keV - 30 keV injection energy for pulse durations up to 2 seconds [4, 5]. This injector has allowed achieving ion temperatures up to near 3.5 keV, which would have been impossible with ECH alone [5,6]. For the purpose of investigating energetic particle modes [2] and confinement in plasmas with near-zero momentum input and hence low toroidal rotation (as expected for ITER), a second 1 MW NBI system (NBI2) with 50 keV - 60 keV acceleration energy was commissioned in 2021 [7]. In order to achieve near-zero NBI torque, the injection direction of NBI2 is opposite to that of NBI1. The higher injection energy and the beam-beam collisions between ions from the opposing sources lead to far higher neutron rates than with NBI1 alone, making a very substantial upgrade of the shielding an essential requirement for the operation of the NBI system.

At the relatively modest temperatures of most TCV plasmas heated with deuterium beams, the neutron production of 2.45 MeV D-D fusion neutrons is dominated by beam-plasma reactions. Neutron rate calculations were performed using the heating codes TRANSP-NUBEAM [8] and a version of ORBIS [4], modified to include beam-beam reactions. They show that with experimentally observed plasma parameters, neutron source rates up to 10^{13} n/s can be obtained with NBI1 only. For NBI1 pulse durations of 1 s and injection power 1MW, this can lead to attaining the daily allowed control room dose limit of 4 μ Sv in as little as 5 discharges out of up to 30 possible discharges per day. As a result of the sharp increase of the cross section for the D-D reaction with energy, the beam-plasma neutron rate for NBI2 is ~ 5 times higher than for NBI1 for the same power and plasma parameters. A further increase was expected from beam-beam interactions between fast ions from the two injectors and moving in opposite directions.

As the TCV hall currently has no ceiling, a large fraction of neutrons escaping vertically are back-scattered from the concrete roof above back down to all locations within the building. In order to allow operation of both NBI sources simultaneously

with full specifications, the publicly accessible rooms in the TCV building, such as the control room, the neutron dose needs to be reduced by at least two orders of magnitude. A classical shielding solution using a concrete ceiling and thicker concrete walls was excluded because the weight of the concrete would exceed the design specifications for the foundations of the TCV shielding walls. Instead, a solution based on polythene (PE), which is 8.7 times more effective by weight than TCV concrete for slowing down fusion neutrons, was developed (i.e. the PE mass required for equivalent shielding is 8.7 times lower than for TCV concrete). The additional shielding requirements are satisfied by a 35 cm thick PE ceiling and a 20 cm thick PE cladding inside the walls of the TCV experimental hall. The specifications for this novel solution for protecting from neutron radiation have been established with the help of neutron transport calculations using a state-of-the-art hybrid (deterministic/stochastic) particle transport methodology. It combines the ADVANTG [9] code to determine efficient variance reduction parameters based on a rough deterministic transport simulation followed by a high-fidelity continuous energy stochastic particle transport simulation using MCNP [10].

II. Radiation protection at the TCV facility

The maximum daily radiation dose for staff and visitors adopted for the TCV facility is 4 μSv based on article 22 of the Swiss federal ordinance on radioprotection [11], which specifies a maximum dose of 1 mSv per calendar year for members of the public. The Swiss Plasma Center has made the choice that all staff members should be regarded as members of the public insofar as radiation safety is concerned, obviating the need for individual dosimetry. In order to simplify access management, the 4 μSv daily limit is also applicable to any areas accessible by staff or members or the public and excludes only areas where any human access is prohibited due to electrical hazard, i.e. the high voltage power supply rooms at the Eastern side of the building and the TCV hall itself. This limit applies whether these areas are occupied or not. Ambient dose levels are routinely measured in the control room (position A in fig.1) and at the platform supporting the gyrotrons (position g).

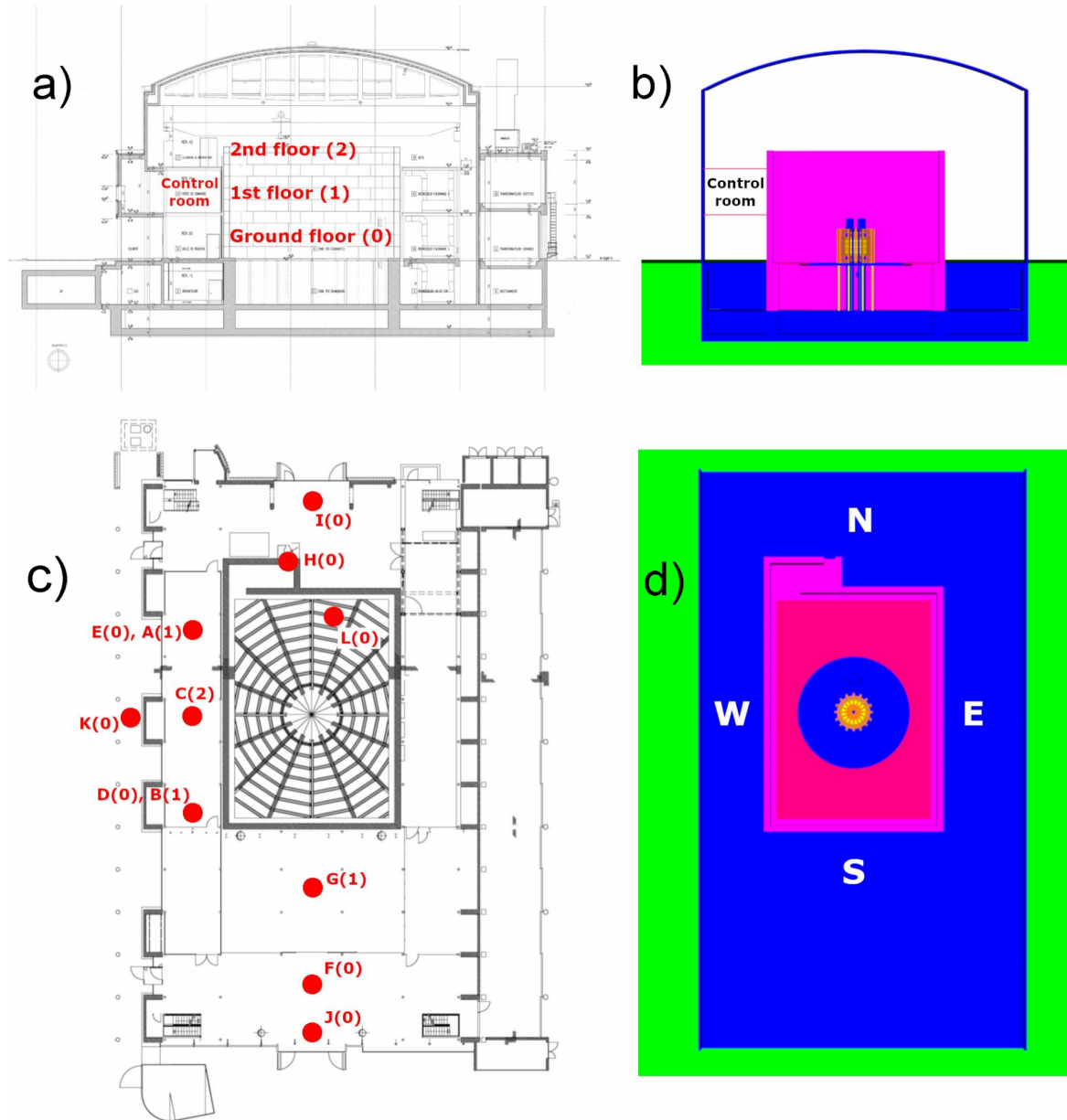


Fig.1. a) East-West engineering cross section of the TCV building in its current conditions. b) East-West cross section of TCV building in MCNP model. c) Horizontal cross section of the TCV building with dose measurement positions (identical with MCNP tally locations). The numbers in brackets indicate the floor levels of the tally locations. The TCV device is at the centre of the TCV hall, on the web-like segmented dismountable ground floor. d) Horizontal cross section of MCNP model.

Fig. 1 shows four cross sections of the TCV building, comparing the construction drawings to the simplified model for Monte Carlo simulations. The TCV hall walls are mostly constituted of $2\text{ m} \times 1\text{ m} \times 0.5\text{ m}$ sized blocks made from barite concrete. A horizontal cross section is shown in figs. 1 c) and d). The TCV device is positioned at the centre of the hall at a height of 1.4 m above the ground level (level 0). Neutron dose measurements are made using three available LUPIN 5401 BF3-NP PSI dosimeters [12] at 12 locations using reproducible TCV pulses with NBI1

operation. Gamma doses are measured using a NAUSICAA probe from the same manufacturer [13]. These dosimeters are designed to have a response approximating the ICRP H*10 ambient dose equivalent [14], i.e. to be representative of the effect of neutron and gamma radiation on biological tissue.

Radiation levels have been measured in 2021 at multiple positions in the building in reproducible discharges with NBI heating using the available NBI1 injector. The positions of the dose measurement and MCNP tally locations are indicated by red dots in fig.1c). They are all at a height of 1 m above the respective floor levels. Table I shows the neutron and the gamma ray doses obtained at the measurement locations in columns 3 and 4, denoted L213 and N227. One of the neutron dosimeters, denoted L214 in table 1, was used as a fixed monitor at position A in the control room. Although these pulses were designed to be reproducible, the pulse-to-pulse variations of the neutron doses were more than 20%, reflecting variations of the TCV neutron source. In order to compensate for these pulse-to-pulse variations, the raw measurements using the mobile neutron probe (L213) were normalised to ones obtained with the reference probe such that $L213^* = L213 / (L214 / \langle L214 \rangle)$ where $\langle L214 \rangle$ is the mean value of all L214 measurements. The normalised measurements are shown in the column denoted L213* in table 1.

TCV Shot #	tally point #	L213 (n°) [uSv] mobile	N227 (γ) [uSv] mobile	L214 (n°) [uSv] fixed at A	L213* [uSv] normalised
70181	A	0.35	0.04	0.35	0.41
70180	B	0.245	0.03	0.32	0.32
70070	C	3.8	0.14	0.458	3.41
70188	D	0.07	0.017	0.39	0.074
70186	E	0.09	0.02	0.395	0.094
70190	F	0.15	0.012	0.39	0.16
70183	G	0.67	0.038	0.385	0.72
70197	H	0.95	0.048	0.44	0.89
70074	I	0.39	0.02	0.47	0.34
70192	J	0.162	0.011	0.4	0.17
70195	K	0.017	0.044	0.42	0.017
70588	L	54.5	0.79	0.52	43.2

Table I: Neutron and gamma dose measurements in a series of reproducible TCV pulses at different tally locations in the TCV building.

Outside the TCV hall, the highest neutron dose rates in the building are obtained at level 2 (position C, 3.8 μSv/s), at the level 0 entrance labyrinth (position

H, 0.95 $\mu\text{Sv/s}$) and at the platform supporting the gyrotron of the electron cyclotron heating system (position G, 0.67 $\mu\text{Sv/s}$). The lowest dose was measured at the ground floor below the control room (position D, 0.07 $\mu\text{Sv/s}$). The control room dose rates (positions A & B) were in the range 0.32 $\mu\text{Sv/s}$ - 0.52 $\mu\text{Sv/s}$. Prompt gamma doses are typically 4 to 50 times lower than the neutron doses. Because of the high doses at level 2 (position C) and on the gyrotron platform (position G), these areas are currently off-limits during NBI operation. NBI operation is terminated for the day when a total dose of 4 μSv is obtained in the control room, sometimes limiting NBI operation to as few as 5 pulses.

Exposure to delayed gammas inside the TCV hall due to activation of machine parts, equipment and the walls following TCV pulses has so far not been a concern. Measurements of the post pulse gamma dose show that for every 1 μSv of total dose measured in the control room, 0.06 μSv of gamma dose is measured in the immediate vicinity of the tokamak. Half of the gamma dose is measured in the first two minutes after a TCV pulse. Since it takes 2 minutes to electrically isolate the TCV device from the high voltage power supplies before entry is permitted, a person spending the whole time between pulses after those first 2 minutes, would be exposed to a gamma dose of 0.24 μSv until NBI operation must be discontinued for the day. The higher post-pulse gamma doses expected in the TCV hall when both beams will operate together will however lead to access restrictions, which will be defined based on gamma dose rate measurements.

III. Modelling of the TCV neutron source

A series of experiments using NBI1 was performed in 2020 as a basis for modelling calculations aimed at estimating the future neutron rates using both NBI sources and hence the shielding requirements. They included a density scan with volume averaged electron densities in the range $1.1\text{--}5.5 \times 10^{19} \text{ m}^{-3}$, two power levels, 0.47 MW and 0.97 MW and two plasma currents, 220 kA and 350 kA.

III.A Calculations for neutron rates with a single neutral beam

Calculations using the codes TRANSP [8] and the much simpler slowing down orbit code ORBIS [4] were performed in 2020 using NBI1 operating at energies in the range 19 keV - 25 keV depending on power requested. A NUCSAFE monitor [15] was used for time resolved, albeit uncalibrated, neutron rate measurements. In the implementation used, ORBIS takes account only of shine-through and first orbit losses, but includes a calculation of the beam-beam neutron rates. The electron temperatures and densities for these calculations were obtained from laser Thomson scattering [16]. There was no available ion temperature measurement. For use in TRANSP, the ion temperatures were estimated using the ASTRA code [17] and an ad-hoc transport model, with T_i/T_e ranging from 0.8 to 2.4 depending on conditions.

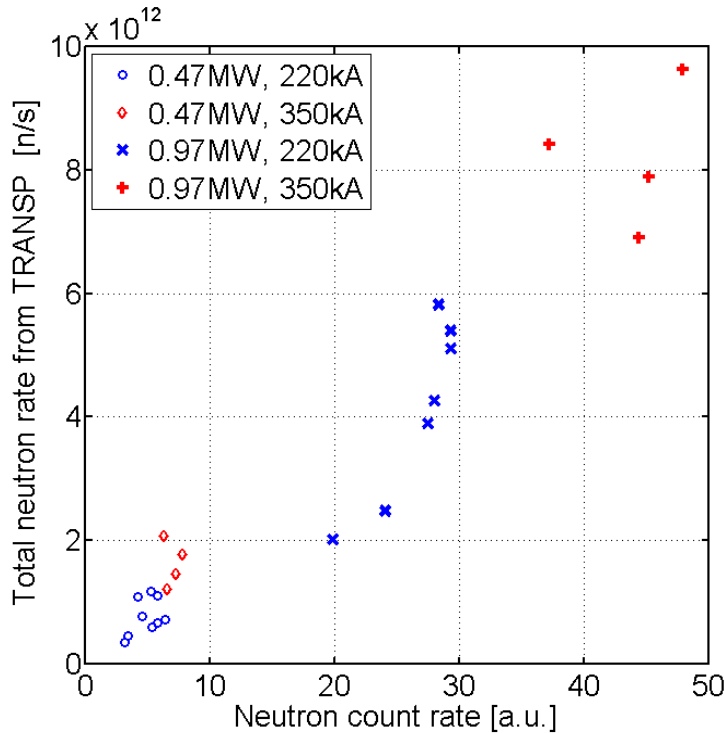
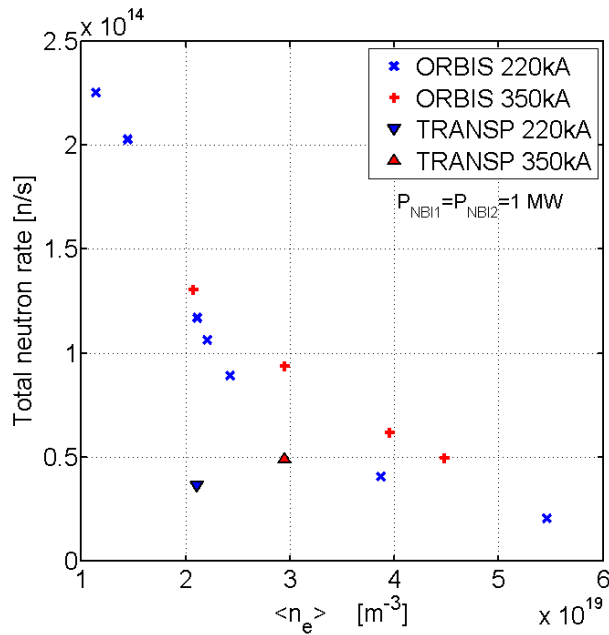


Fig.2. Neutron rates calculated by TRANSP vs the uncalibrated neutron count rate measured using the Nucsafes 1 detector. The symbols refer to different NBI1 power levels and plasma currents.

For ORBIS, $T_i/T_e = 2$ was assumed in all cases, as this temperature ratio was the highest previously measured by charge exchange spectroscopy [5]. The ion temperature has a modest effect, as thermal-thermal reactions were calculated to be always below 11% of the beam-thermal neutron rate. Plasma rotation in the direction of the injection slightly reduces the beam-thermal neutron rates. As no rotation measurement was available, zero rotation was assumed. TRANSP includes orbit losses during slowing down and most importantly, charge exchange losses, calculated on the basis of the measured vessel pressure. As a result of the neglect of these losses in ORBIS, beam-thermal neutron rates by ORBIS are on average some 20% higher for NBI1 than those calculated by TRANSP. The largest differences, up to 45% of the TRANSP prediction, are seen at the lowest densities where neutrals penetrate farthest into the plasma. At the highest densities, where charge exchange



losses are least important, ORBIS and TRANSP agree within 10%. The highest neutron rates, near 10^{13} n/s were predicted by TRANSP at the highest power (0.97 MW) and plasma current (350 kA) at medium volume average density ($\sim 3 \times 10^{19} \text{ m}^{-3}$). Fig.2 shows that there is a high degree of proportionality between the neutron rates from the uncalibrated NUCSAFE neutron detector [15] and the TRANSP predictions. The higher neutron rates obtained at the higher current level (350 kA) are explained by the better orbit confinement and the higher electron temperatures obtained the higher current.

Fig.3 predictions for neutron rates with NBI1 and NBI2 together, for $P_{\text{NBI1}} = P_{\text{NBI2}} = 1 \text{ MW}$.

III.B Extrapolation of the neutron rates to operation with two neutral beams

The next step was to repeat the modelling, assuming that both NBI1 and NBI2 were operating simultaneously at a power of 1 MW each, with NBI1 counter-injecting (opposite to the direction of the plasma current) with 25 keV acceleration voltage and NBI2 co-injecting (same direction as the plasma current) at 50 keV acceleration voltage. This modelling was not self-consistent, as it was assumed that the densities and temperatures were the same as with NBI1 only. From basic confinement scaling ($W_p \propto P_{\text{tot}}^{0.5}$) and neglecting the ohmic power, the electron temperature may rise by

up to ~40% when the NBI power is doubled, provided the density remains constant. In our experience, however, the density rises and the temperature remains roughly constant when beam power is applied or increased. As a result, the dominant beam-plasma neutron rate, which depends mainly on electron temperature and not on density, is adequately predicted with our assumptions. The predictions for the two codes are shown in fig.3. Only 2 cases at 1MW, those which produced the highest neutron rates in the experiment, were modelled with TRANSP (triangles). Due to the absence of charge exchange neutrals ORBIS predictions for the neutron rates in these two cases are higher by a factor of two. The TRANSP and ORBIS calculations for the 350 kA case with $\langle n_e \rangle \approx 3 \times 10^{19} \text{ m}^{-3}$ show that neutron rates with both beams are respectively 5 times and 10 times above those with NBI1 only. The neutron rates include a substantial contribution from beam-beam reactions from reactions between the ion populations from NBI1 and NBI2, which at birth have relative energies up to 145 keV (assuming injection energies of 25 and 50 keV). In the case of the ORBIS calculation, the beam-beam contribution was about half of the total neutron rate for $\langle n_e \rangle \approx 3 \times 10^{19} \text{ m}^{-3}$. Initial short pulse (~50 ms) operation in 2021 has confirmed that the neutron rates with both beams can exceed those from NBI1 by an order of magnitude.

There is a clear inverse relation of ORBIS predictions with density (fig.3) as the fast ion densities scale as $n_f \propto T_{\text{slow}} \propto n_e T_e^{3/2}/n_e$ and hence for the beam-beam neutron rate $R_{\text{nbb}} \propto n_f^2 \propto P_{\text{NBI1}} P_{\text{NBI2}} T_e^3 / n_e^2$. T_e is seen to scale weakly inversely with density in these discharges, $T_e \propto n_e^{-1/3}$, hence $R_{\text{nbb}} \propto P_{\text{NBI1}} P_{\text{NBI2}} n_e^{-3}$. This simple scaling does not take into account the fact that the beam deposition profile depends on plasma density. The ORBIS predictions at low to medium density ($\langle n_e \rangle < 3 \times 10^{19} \text{ m}^{-3}$) are clearly overestimates for current conditions in TCV, but may be relevant if neutral densities in the plasmas and hence charge exchange losses can be significantly lowered, e.g. by wall conditioning.

III.C Assessment of shielding requirements

We conservatively assume, based on the ORBIS predictions for $\langle n_e \rangle \approx 3 \times 10^{19} \text{ m}^{-3}$ and $I_p = 350 \text{ kA}$ shown in fig.3, that the neutron rates can be up to 10^{14} n/s when both NBI's are operated together, i.e. 10 times higher than with NBI1 alone. We also assume that the pulse duration, now typically 1 s, can be as long as 2 s. We use the current worst conditions for NBI1 operation, which limit the daily operation to 5 pulses (out of a technically possible 30 pulses) as a scaling basis. In order to remain within the daily radiation dose limit for 30 consecutive pulses with highest expected neutron rates, for the longest possible duration and for 30 pulses per day, the shielding needs to reduce the radiation dose by a factor 120. We note that it is very unlikely that 30

worst case pulses would actually be performed on a single experimental day and much less so that such worst case experimental days would be performed on every day of the year.

IV. Shielding material studies

First, several types of concrete as well as borated and un-borated polythene (PE) were assessed for their suitability as materials for additional shielding. The types of concrete include the barite concrete used for the existing side walls of the TCV hall, ordinary concrete and a handful of promising concrete types selected from the Pacific NorthWest National Laboratory (PNNL) Compendium of Material Composition Data for Radiation Transport Modelling [18] for their high hydrogen and boron content. TCV concrete has a density of $3.4 \times 10^3 \text{ kg/m}^3$ and contains 50.8 % barium by weight. By comparison, ordinary concrete has a density of $2.4 \times 10^3 \text{ kg/m}^3$. Two of the concrete types in the PNNL compendium [18] have a modestly higher neutron moderating power than TCV concrete for a similar mass density (no 87 & 88 in the compendium). However a concrete based solution, which would have implied doubling the wall thicknesses and building a 70 cm - 90 cm thick concrete ceiling had to be abandoned because the foundations of the TCV hall walls had only been specified for barite concrete walls up to 1 m thickness, but no ceiling. An additional constraint was the capacity of the overhead crane in the TCV building, which is limited to 10 tons and is therefore too low for a demountable ceiling made of 15 m long heavy concrete beams of practical cross section.

IV.A Spherical model for material comparisons

In order to compare the dose attenuation properties of different materials a simple spherical model with the source inside was devised. The simulation was performed with a hollow sphere with different thicknesses of the wall and a doughnut shaped neutron source similar to a TCV plasma. For each of the studied wall configurations a MCNP simulation using the MCNP5 v1.60 [10] together with FENDL 3.1d [23,24] nuclear data library was performed using 10^8 source particles to ensure the statistical uncertainty of the results was below 1 %. Fig. 4 shows the relative flux averaged over the surface of the sphere per 2.45 MeV source neutron penetrating shieldings of various thicknesses of some of the materials which were under consideration. We can see that for neutron shielding PE based solutions perform vastly better than concrete. Polythene (PE) is one most effective solid materials for neutron moderation by weight that is available in bulk. A 20 cm thickness of PE has a neutron moderating power equivalent to 50 cm of TCV barite concrete for an 8.7 times lower weight (materials only, without iron reinforcements or support structures). Two of the PE based shields calculated were laminates with the last 2.5, respectively 5 cm of ordinary PE replaced by PE doped with 5% of boron (labelled SWX 201 in fig.4) [19]. Boron has an exceptionally high neutron capture cross section at energies

below 1eV. Fig.4 shows that the two laminates perform better than pure PE and doped PE. It also shows that 20 cm of PE is equivalent in neutron attenuation to 50 cm of barite concrete.

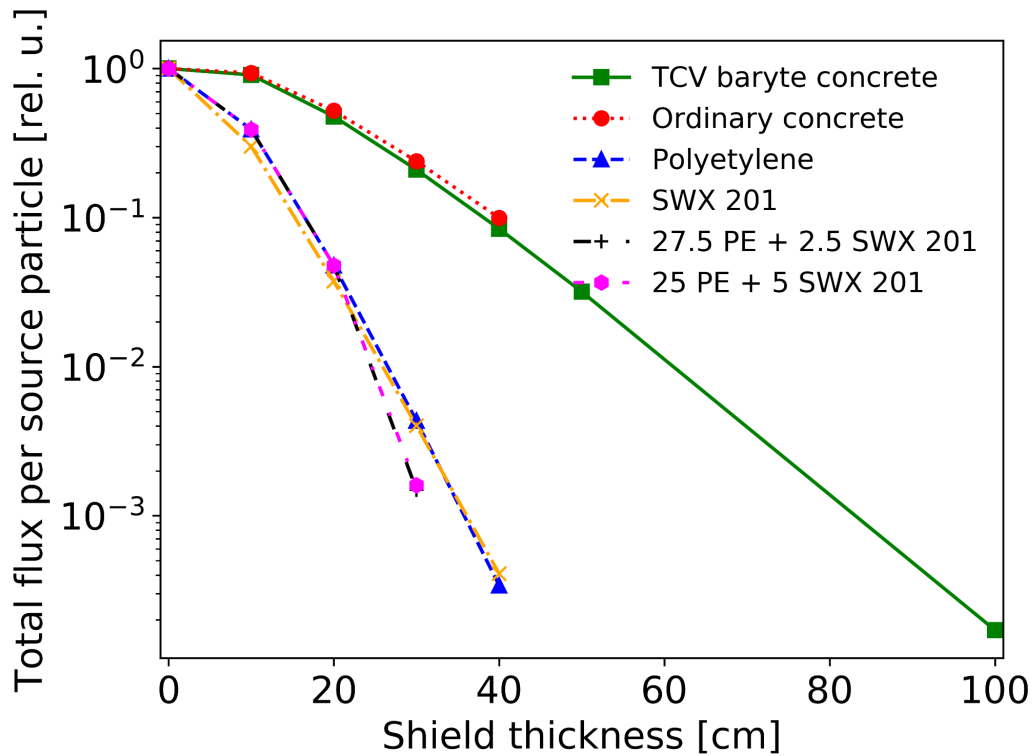
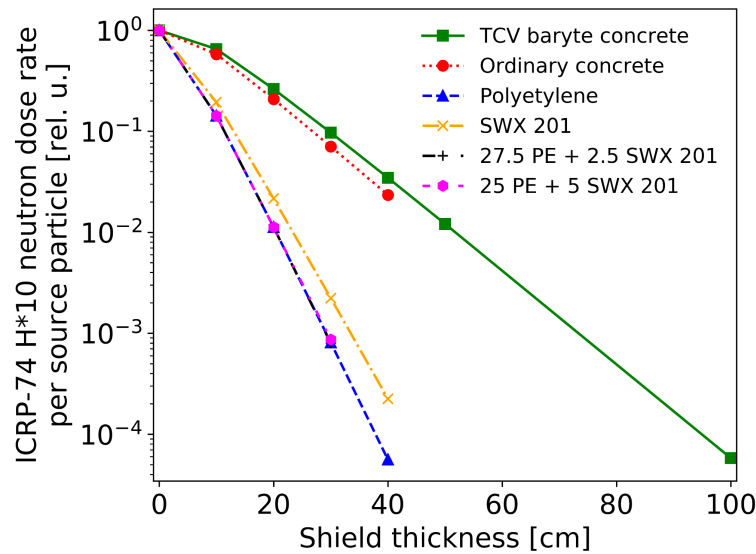


Fig.4. Neutron flux per source particle in dependence of the position in the shield for different PE and SWX laminates and two types of concrete, calculated using the simple spherical model.

Fig.5 shows the dose rates corresponding to the fluxes in fig.4. The ambient dose equivalent is defined as $H^*(10) = \int \Phi(E) h^*(10) dE$, where the integral extends over the entire spectrum [14]. The spectral weighting factor, $h^*(10)$, represents the energy dependent detrimental biological effects of neutron radiation. The presence of boron in PE makes virtually no difference to the neutron dose rate, as the neutrons removed by capture by the boron are all of low energy (<1 eV) and hence contribute little to the H^*10 ambient dose equivalent. This can be understood by inspecting the neutron spectra transmitted through the shields, shown in fig. 6. The vertical axis is the flux per unit lethargy $f(u) = E\Phi(E)$, where Φ is the flux in neutrons/s/cm and $u = \ln(E_0/E)$ is called the neutron lethargy and $E_0 = 2.45$ MeV is the neutron energy at the source. The unit lethargy spectral interval is an interval of energy $[E_1, E_2]$ such that $E_2/E_1 = e$. We see that above a few eV all spectra are similar and the spectra of the three PE based shields are essentially identical. The two boron laminates remove the large spectral peak in the thermal region (from $\sim 10^{-2}$ eV to $\sim 10^{-1}$ eV). This narrow region has very little weight in comparison with the wide high energy part of the spectrum. In addition to the much greater spectral width of the high energy part, the spectral weighting factor $h^*(10)$, rises sharply for $E > 1$ keV and is ~ 30 times larger for $0.7 \text{ MeV} < E < 5 \text{ MeV}$ than in the thermal range. This means that even after

substantial attenuation, the ambient dose from a fusion neutron source remains dominated by energetic neutrons and the shielding needs to be optimised for fast, rather than for thermal neutrons. However, when large dose attenuation factors are required, as is the case with TCV, gamma ray transmission and gamma ray emission following neutron capture in the shielding materials have to be accounted for too. The advantage of boron doped PE is that most of the captured neutrons lead to the emission of a gamma photon with 0.5 MeV energy, whereas capture by hydrogen, the main capture process in pure PE, leads to the emission of a 2.1 MeV photon, which is more difficult to stop and is associated with a higher dose. The gamma ray contribution was evaluated in the full building model described in section VI.



*Fig.5 Neutron H^*10 ambient dose equivalent per source particle in dependence of the position for different PE and SWX laminates and two types of concrete, calculated using the simple spherical model.*

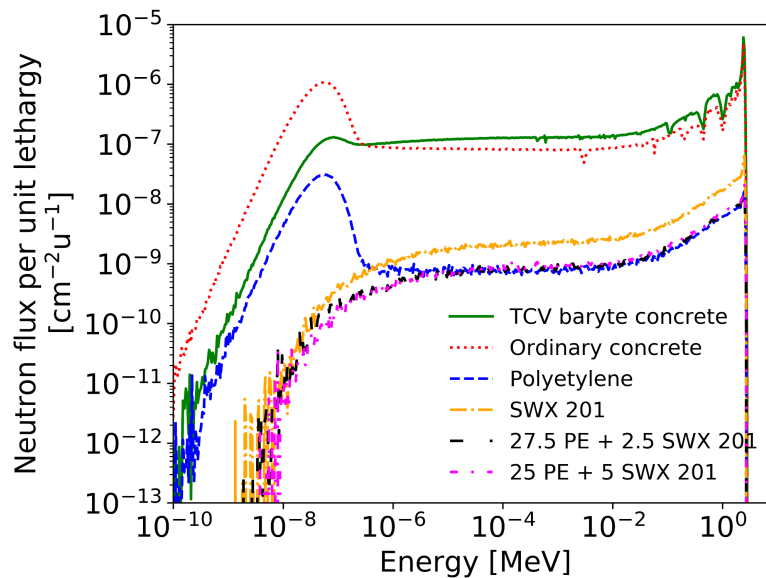


Fig.6. Neutron lethargy spectra in 640 energy groups after 30 cm for different PE and SWX laminates and two types of concrete calculated using the simple spherical model. The spectra are given in units per source particle.

IV.B Experimental characterisation of polythene as a shielding material

Before committing several million Swiss francs to this project, the neutron dose attenuation by PE was experimentally tested for thicknesses up to 30 cm using a set of six nestable PE boxes made from 5 cm HD PE 500 sheets [20]. The four innermost boxes are depicted in fig.7 without the 5 cm thick PE lids. A mobile dosimeter was placed inside the innermost box and the boxes were closed with the lids for the measurements. The boxes were placed in the TCV hall with one side facing the TCV device at a distance of 7 m. Measurements were made for different total thicknesses of PE in a series of reproducible TCV discharges with NBI1 and normalised to measurements by a reference detector. Fig.8 shows the measured attenuation, together, for comparison, with the MCNP predictions for the spherical model, demonstrating that a dose reduction by a factor >3000 is obtained with 30cm of PE.

This result validated the choice of PE as a neutron shielding material and exceeded the expectations based on the spherical model. The nearly exponential decrease of the dose with thickness may be expressed by an effective dose attenuation coefficient of PE, which amounts to 29 m^{-1} for the experimental result and 24 m^{-1} for the calculations with the spherical model. The former is likely an overestimate due to the geometry of boxes because detected neutrons incident onto the sides of the boxes experience a higher effective thickness.

The experiment was repeated, for a PE thickness of 20 cm, using the NAUSICA gamma dosimeter. Prompt gamma emission is detected without the PE box, originating from neutron capture in the walls and equipment in the TCV hall. The gamma dose measured inside the box was only a factor 1.77 lower than without the box. We conjecture that the gammas detected consisted in part of attenuated gammas incident onto the assembly and of gammas produced by neutron capture in the PE. Future MCNP calculations are to determine what fraction of the gamma dose inside the box is due to neutron capture in PE.



Fig.7 Photograph of the four innermost PE boxes (without their lids) used for experimental measurements of neutron and gamma ray dose attenuation.

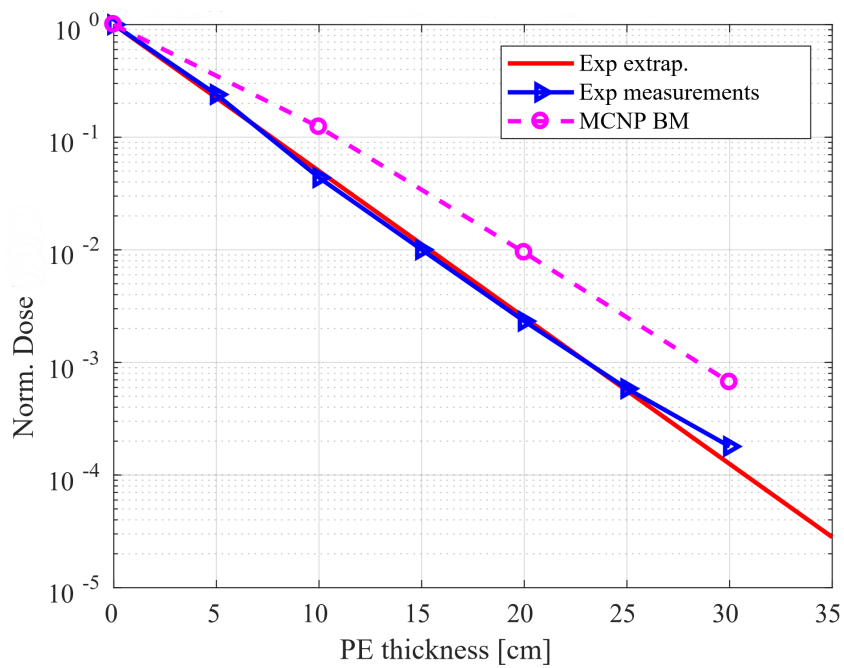


Fig.8 Measured normalised dose vs shielding thickness (blue triangles), lin-log fit and expectations from spherical MCNP model (broken lines).

V. Design and modelling of the TCV radiation shielding

The MCNP shielding models and the engineering design progressed hand in hand, the latter being subject to many supplementary constraints. A detailed description of the final MCNP model is available in ref. [21]. These include the weight limit (10 tons) of the available overhead crane, the requirement to use non-magnetic steel support beams for supporting the PE ceiling, room for a light (1 ton) overhead crane below the PE ceiling, accessibility, fire safety, ventilation and safety requirements for the installation and removal of the ceiling elements. A basic previous neutronics model of the building, provided in 2016 by CCFE on a commercial basis, was upgraded in steps to include a model of the TCV device with a steel vessel and copper coils, to provide a better representation of the neutron and gamma spectra produced by the device. Some of the major structures in the TCV hall, the TCV hall floor (partly made of wood and partly of concrete) and of the 10 cm thick wooden floors between levels 0, 1 (control room) and 2 (storage area) were included for better realism. More recently, far more details of the building, including the equipment in the vicinity of the TCV device and the structure of the roof were included in the model. This provided a substantial improvement between the predicted and measured doses throughout the building [21].

Initial shielding designs had all or part of the wall PE shielding on the outside of the wall for simplicity and accessibility (requiring less equipment to be removed from the inside walls). The MCNP [10] calculation showed that this is satisfactory for neutron dose attenuation, but not for the gamma doses. The current design therefore has all of the PE wall shielding adjacent to zones accessible during TCV pulses on the inside, allowing most of the gammas to be stopped by the barite concrete walls. The height of the concrete wall had to be reduced by 1.5 m to allow access with the overhead crane because of the extra thickness of the ceiling and supporting structure. The concrete blocks recovered will be re-used as additional shielding at the lower part of the hall, up to a height of 3 m in parts of the hall, as their neutron shielding is equivalent to that of 20 cm of PE (PE will be used above the concrete blocks). The hall is topped by a 35 cm thick PE ceiling and no further gamma shielding. The PE covered areas will total 800 m² for a total weight of 200 tons. Construction started in February 2023 and was expected to take several months.

Fig.9 shows a North-South cross section of the junction of the ceiling and the supporting concrete walls at the South of the hall. The PE slabs rest on eleven 50 cm high beams spaced 2 m apart, which themselves rest on a pair of 30 cm high beams placed on 20 cm thick PE above the East and West walls. Radiation shielding in the horizontal direction is provided by a total of 30 cm of PE and a parapet made of 20 cm of barite concrete. The latter is essential to stop the majority of the gammas produced by neutron capture inside the PE. An equivalent arrangement, from the

point of view of neutron and gamma shielding, exists at the junctions of all 4 walls with the ceiling.

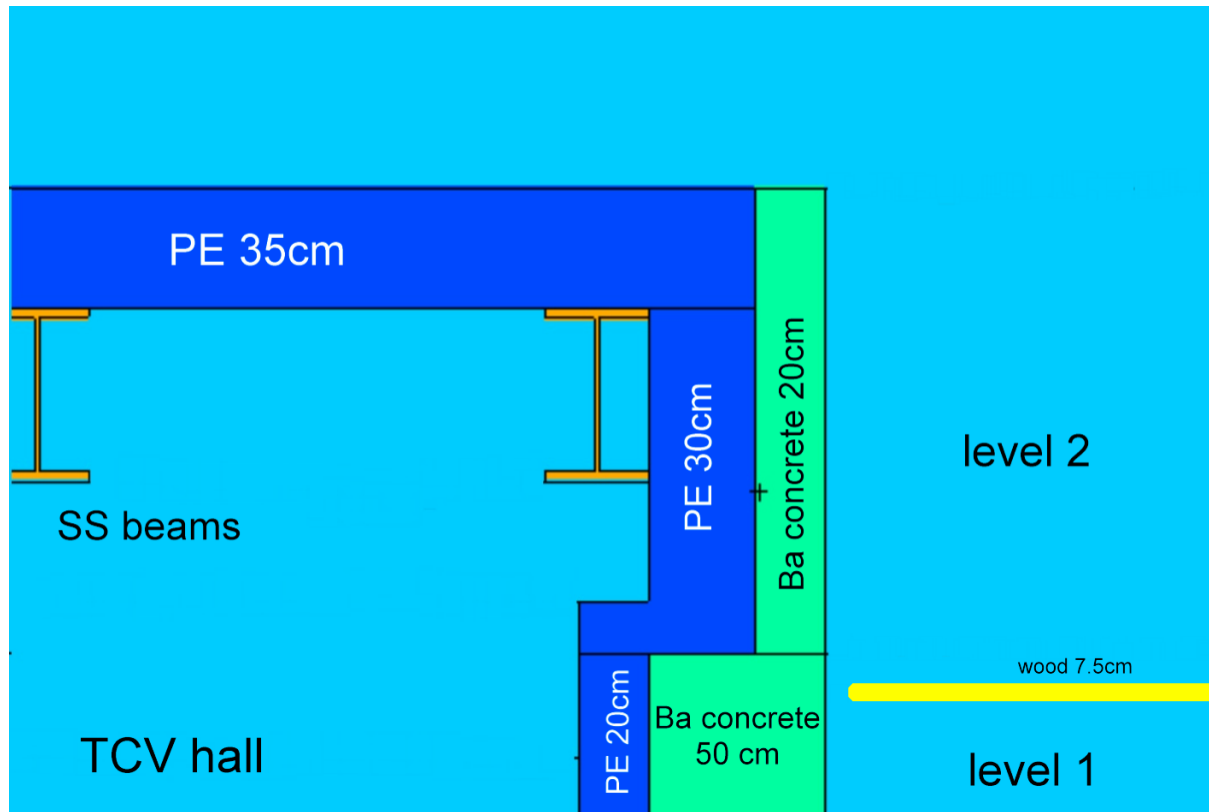


Fig.9. Junction of ceiling and the 50 cm thick South wall of the TCV experimental hall (North-South cut through the middle of the hall). The 20 cm thick barite concrete side wall (parapet) at level 2 is necessary for the reduction of gamma doses at levels 1 and 2 produced by neutron capture in the PE neutron shielding at level 2.

The hall entrance at the North-West corner will be widened to 3 m and equipped with a custom made sliding door consisting of two 17.5 cm thick boron doped PE sheets. The remainder of the entrance above a height of 3 m and up to the ceiling will be made of vertically stacked boron doped PE slabs totalling a thickness of 35 cm that must be light in order to be easily removable for transferring large pieces of equipment. Boron doped PE was chosen for these locations in order to reduce gamma ray doses, as, because of weight restrictions, there is no additional gamma ray shielding by high atomic mass materials. At level -1, the barite walls are 1 m thick and no PE cladding is needed. However there are numerous passages in the East and West walls, approximately 50x50 cm wide for power and signal cables. All of these will be plugged with a thickness of at least 40 cm of PE or filled with PE beads. Access to the TCV hall at level -1 is granted by a sliding boron doped PE door similar to the one at level 0. The ceiling is made from 2 overlapping layers of PE slabs, 17.5 cm thick, 6 m long and 2 m wide and will be supported by 15 m long steel

beams spaced by 2 m and oriented in the East-West direction. As non-magnetic steel beams are not standard products, they will be made by welding austenitic type 1.4307 steel sheets together with cross sections equivalent to that of standard beams [22].

VI. MCNP validation of the engineering design

The MCNP engineering model includes, in addition to the detailed features of the building and the contents of the TCV hall, all essential features of the engineering design, i.e. the structural elements such as the beams and realistic models of the sliding doors. All simulations were performed with MCNP5 v1.60 [10] together with FENDL 3.1d [23,24] nuclear data library and ADVANTG 3.2.1 [9] for production of variance reduction parameters for tally position located behind different walls of the TCV building. The neutron source intensity used in simulations was 4×10^{13} neutrons per second. East-West cuts of the calculated neutron dose rate fields for unshielded and shielded conditions are shown in figs 10 and 11. The corresponding gamma radiation fields are shown in figs 12 and 13.

An initial calculation without the concrete parapet shown in fig.9 established that neutron doses were at or below the design targets throughout the TCV building. However, gamma doses at level 2 (tally point C in fig.1), at the gyrotron platform (G) and in the control room were (A & B) substantially exceeded the design objectives. At tally point C, the gamma dose exceeded the design target by a factor 11. In a subsequent set of calculations the origin of the gammas was determined by defining particular parts of the PE shielding suspected of being major contributors to the gamma ray doses in the inhabited zones as “cells”. The gamma ray “importance” of the cells was set to 0, meaning that all gamma rays entering or generated in the cell would be absorbed. In this way, combinations of calculations using different cells with importance set to 0 were used to determine the contributions of the various parts of PE shielding to the dose rates at the tally points. The results established that the majority of the gammas contributing to the doses at the tally locations were indeed emitted by the PE side walls at level 2. This prompted the addition of a 20 cm thick barite concrete parapet at level 2 as shown in fig.9. The calculations also showed the contribution of gammas emitted by or reflected from the ceiling is low, obviating the need for gamma ray shielding on top of the ceiling.

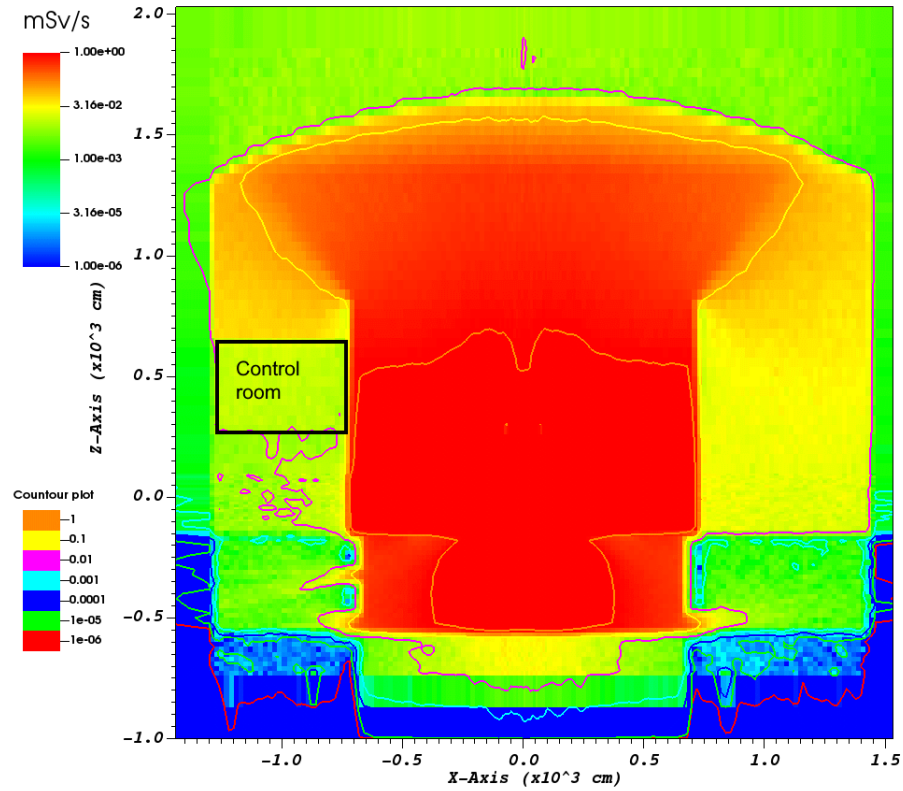


Fig.10. Neutron dose rate distribution for an East-West cut through the TCV building for an MCNP model reflecting current conditions.

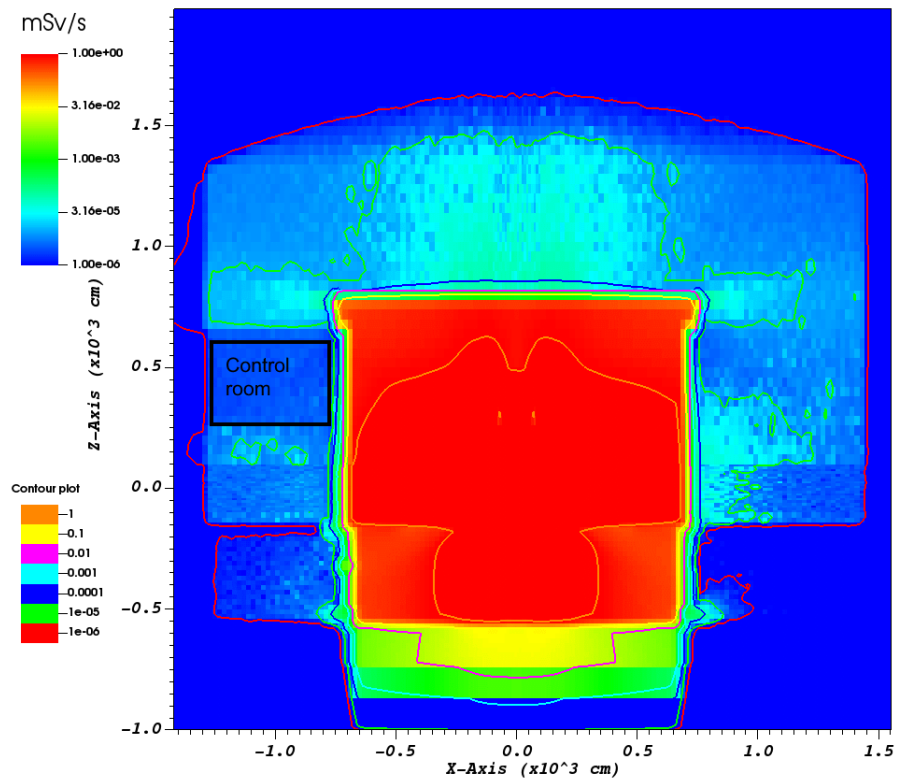


Fig.11. Neutron dose rate distribution for an East-West cut through the TCV building for an MCNP model with proposed shielding.

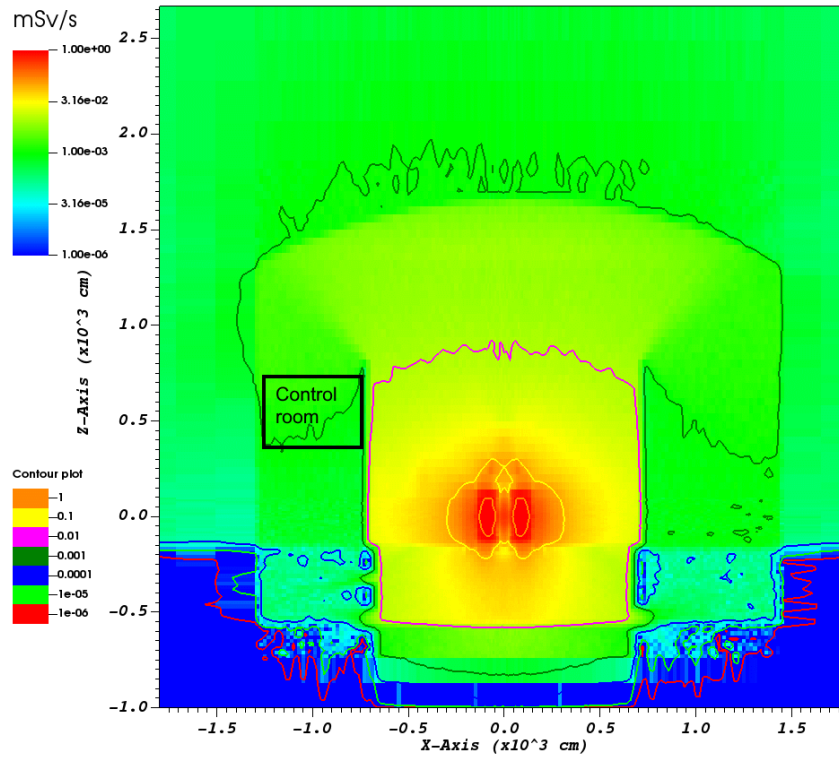


Fig.12. Gamma dose rate distribution for an East-West cut through the TCV building for an MCNP model reflecting current conditions.

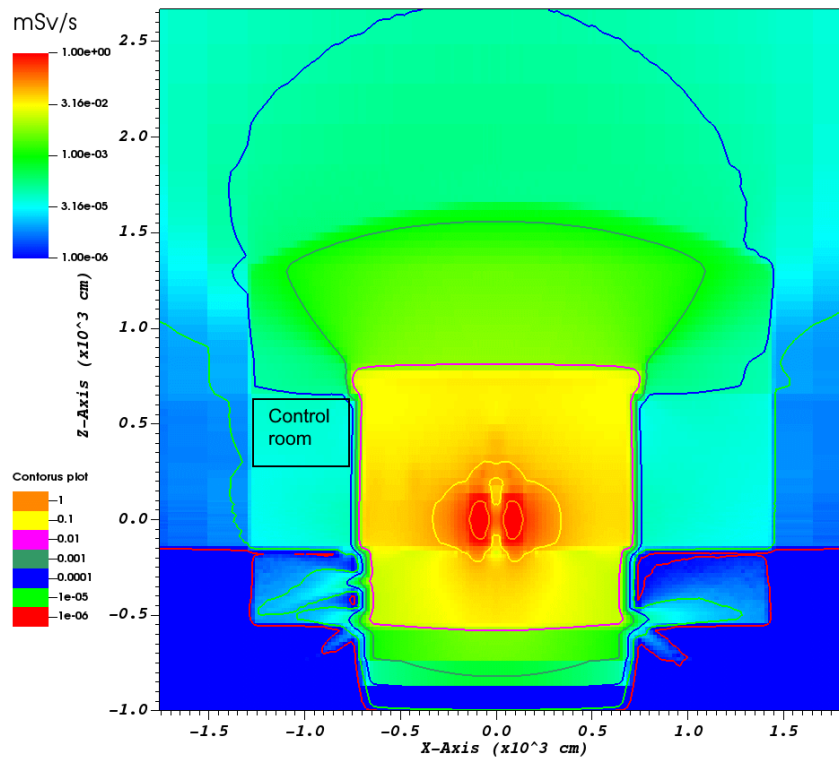


Fig.13. Gamma dose rate distribution for an East-West cut through the TCV building for an MCNP model with proposed shielding.

Tables II and III show the expected dose reductions for, respectively, neutrons and gammas at the various tally points for a source rate of 4×10^{13} n/s. The columns denoted 'reference model' refer to the model of the TCV building without additional shielding. The results of the calculations are subjected to a normalisation to the experiment dose measurements for evaluating the highest expected daily dose expected for 30 pulses of a duration of 2 seconds and a neutron yield 10 times higher than with NBI1 only. The magnitude of the source rate therefore has no influence on the calculation of the expected highest daily dose. The relative uncertainties for the doses are determined by the Monte Carlo statistics. We see that in the control room (A & B) and the gyrotron platform (G) the target dose reduction is met, with a total highest expected daily dose near or below 4 μ Sv. At level 2 however (tally point C), the highest expected total daily dose (neutrons + gammas) is 11.2 μ Sv, i.e. almost a factor 3 above the maximum allowed daily dose, implying the necessity of access management. This, however, is deemed tolerable, as level 2 is a storage area requiring only occasional access and the achievement of highest expected daily doses is considered to be exceptional.

Table II: Calculated neutron H*10 dose rates for the engineering design for a source rate of 4×10^{13} n/s.

Location		Reference model		Reference + PE shield model		Rel. dose reduction	Highest daily dose
	Loc.	Dose [mSv/s]	Rel. unc. [%]	Dose [mSv/s]	Rel. unc. [%]		μ Sv
Control room, North	A	1.03E-02	3.0	5.86E-06	4.1	1757.82	0.35
Control room, South	B	9.94E-03	2.9	3.26E-06	5.3	3046.84	0.20
2 nd floor	C	5.37E-02	1.3	2.42E-05	1.8	2219.83	1.45
Workshop	D	5.18E-03	4.0	4.69E-06	4.6	1105.37	0.28
Diagnostic lab	E	5.66E-03	4.3	1.27E-05	3.0	446.48	0.76
South 'extension'	F	5.30E-03	4.0	1.68E-06	7.5	3146.45	0.10
Gyrotron platform	G	1.62E-02	2.3	3.11E-06	5.6	5213.46	0.19
TCV entrance turnstile	H	1.07E-02	3.8	1.26E-05	3.8	849.57	0.76
North door	I	8.98E-03	3.2	3.61E-06	5.7	2487.87	0.22
South door	J	5.04E-03	4.1	1.46E-06	8.6	3461.35	0.09
West side outside	K	5.91E-04	5.6	1.47E-06	9.2	401.43	0.09
TCV hall	K	6.42E-01	0.4	8.61E-01	0.1	0.75	5.16E+4

Table III: Calculated gamma H*10 dose rates for the engineering design for a source rate of 4×10^{13} n/s.

Location		Reference model		Reference + PE shield model		Rel. dose reduction	Highest daily dose
	Loc.	Dose [mSv/s]	Rel. unc. [%]	Dose [mSv/s]	Rel. unc. [%]		μ Sv
Control room, North	A	6.23E-04	2.4	3.33E-05	0.3	18.71	2.00
Control room, South	B	6.37E-04	2.5	2.10E-05	0.3	30.35	1.26
2 nd floor	C	1.65E-03	1.5	1.62E-04	0.2	10.16	9.75
Workshop	D	4.66E-04	3.0	1.11E-05	0.5	42.00	0.67
Diagnostic lab	E	3.70E-04	3.3	2.28E-05	0.4	16.22	1.37
South 'extension'	F	3.57E-04	3.4	7.95E-06	0.4	44.90	0.48
Gyrottron platform	G	8.65E-04	2.2	3.82E-05	0.3	22.62	2.29
TCV entrance turnstile	H	2.41E-04	5.1	6.16E-05	0.3	3.91	3.69
North door	I	3.76E-04	3.2	2.23E-05	0.3	16.85	1.34
South door	J	3.24E-04	3.5	8.82E-06	0.5	36.75	0.53
West side outside	K	1.06E-04	6.2	6.32E-06	0.9	16.76	0.38
TCV hall	L	1.02E-02	0.67	2.38E-02	0.01	0.43	1.42E+3

7. Conclusions

The current work has established that a retrofit polythene shielding of the TCV hall satisfies the stringent requirements of a total neutron and gamma dose reduction by a factor 120. We emphasise that this is a conservative figure and we regard it as very unlikely that TCV would regularly produce daily neutron doses requiring such a high level of additional protection. While the use of polythene allows weight savings of a factor 8.7 compared to barite concrete for neutron shielding, it cannot be used on its own if it is in direct view of human occupied zones, because neutron capture by hydrogen in the material leads to significant gamma emission. Gamma emission must be stopped by a high atomic charge material such as barium. This required the addition of a 20 cm thick parapet made from barite concrete on top of the side walls where naked PE would otherwise be in direct view. However, we found that it is

acceptable not to cover the polythene ceiling of the TCV hall with a gamma ray stopping material, as the top of the ceiling is not in direct view from any human accessible zone and the roof above the ceiling is a weak contributor to the gamma emission. Following implementation of the radiation shield in 2023, a series of experiments will be undertaken to experimentally validate the design and the protection level afforded.

Acknowledgements

This work has been carried out in part within the framework of the EUROfusion Consortium, funded by the European Union via the Euratom Research and Training Programme (Grant Agreement No 101052200 — EUROfusion). Views and opinions expressed are however those of the author(s) only and do not necessarily reflect those of the European Union or the European Commission. Neither the European Union nor the European Commission can be held responsible for them.

The JSI team acknowledges the financial support from the Slovenian Research Agency, research core funding No. P2-0073 and P2-0405.

References

- [1] H. Reimerdes et al, 2022 *Nucl. Fusion* 62 042018
- [2] B Geiger *et al* 2020 *Plasma Phys. Control. Fusion* 62 095017, <https://doi.org/10.1088/1361-6587/aba19e>
- [3] T.P. Goodman et al, 2003 *Nucl. Fusion* 43 1619, <https://doi.org/10.1088/0029-5515/43/12/008>
- [4] A.N. Karpushov et al, 36th EPS Conference on Plasma Physics, June 29 - July 3, 2009, Sofia, Bulgaria, ECA Vol.33E, P-2.140 (2009) http://ocs.ciemat.es/EPS2009/pdf/P2_140.pdf
- [5] A.N. Karpushov et al, *Fusion Engineering and Design* Volume 123, November 2017, Pages 468-472, <https://doi.org/10.1016/j.fusengdes.2017.02.076>
- [6] M. Vallar et al, *Fusion Engineering and Design*, Volume 146, Part A, September 2019, Pages 773-777, <https://doi.org/10.1016/j.fusengdes.2019.01.077>
- [7] A.N. Karpushov et al, "Upgrade of the neutral beam heating system on the TCV tokamak – second high energy neutral beam", *Fusion Engineering and Design*, 187, 2023, 113384, <https://doi.org/10.1016/j.fusengdes.2022.113384>.
- [8] A. Pankin et al. 2004 *Comput. Phys. Commun.* 159 157-184
- [9] Mosher, Scott W., Aaron M. Bevill, Seth R. Johnson, Ahmad M. Ibrahim, Charles R. Daily, Thomas M. Evans, John C. Wagner, Jeffrey O. Johnson, and Robert E. Grove. "ADVANTG—52 an automated variance reduction parameter generator." ORNL/TM-2013/416, Oak Ridge National Laboratory (2013).
- [10] Kiedrowski, Brian, Thomas E. Booth, Forrest B. Brown, Jeffrey S. Bull, Jeffrey A.

Favorite, R. Arthur Forster, Roger L. Martz, and M. C. N. P. Documentation. "MCNP5-1.6, Feature Enhancements and Manual Clarifications." LA-UR-10-06217 (2010).

[11] Le Conseil fédéral suisse, Ordonnance sur la radioprotection (ORaP) du 26 avril 2017
<https://fedlex.data.admin.ch/filestore/fedlex.data.admin.ch/eli/cc/2017/502/20210101/fr/pdf-a/fedlex-data-admin-ch-eli-cc-2017-502-20210101-fr-pdf-a.pdf>

[12] ELSE Nuclear, via Riccardo Pitteri, 10 - 20134 Milano - ITALY, Technical specifications for LUPIN series neutron dosimeters, <http://www.elsenuclear.com/en/lupin-series>

[13] ELSE Nuclear, via Riccardo Pitteri, 10 - 20134 Milano - ITALY, Technical specifications for NAUSICAA Ion-Chamber-based gamma monitoring units
http://www.elsenuclear.com/media/k2/attachments/DAT_IONCHAMBERDET_EN_1.10.pdf

[14] ICRP, 2007. The 2007 Recommendations of the International Commission on Radiological Protection. ICRP Publication 103. Ann. ICRP 37 (2-4).

[15] Southern Scientific Ltd, Henfield, UK,
<https://www.southernscientific.co.uk/products-by-manufacturer/nucsafe?region=europe>

[16] H. Arnichand *et al* 2019 *JINST* 14 C09013,
<https://doi.org/10.1088/1748-0221/14/09/C09013>

[17] G.V. Pereverzev, ASTRA. An Automatic System for Transport Analysis in a Tokamak.
<http://hdl.handle.net/11858/00-001M-0000-0027-646C-F>

[18] RJ McConn et al, Compendium of Material Composition Data for Radiation Transport Modelling, Pacific NorthWest National Laboratory, USA, 201
https://www.pnnl.gov/main/publications/external/technical_reports/PNNL-15870Rev1.pdf

[19] Shieldwerx spec sheet, <https://www.shieldwerx.com/assets/swx-201hd-2018.pdf>

[20] Eriks Technical Sheet HMW-PE / PE-500
https://eriksdigitalcdn.azureedge.net/hlr-system/maagtechnic/datasheets/technische%20datenblätter/kunststoffe/hmw-pe-pe-500_eng.pdf

[21] M Fortuna et al, Fusion Engineering and Design, 2023, vol 191, 113562,
<https://doi.org/10.1016/j.fusengdes.2023.113562>

[22] 'Dimensions of Steel Beams Type HEB', PIPING-WORLD,
<https://www.piping-world.com/dimensions-of-steel-beams-type-heb>

[23] R. Forrest, R. Capote, N. Otsuka, T. Kawano, A.J. Koning, S. Kunieda, J-Ch. Sublet, and Y. Watanabe, FENDL-3 Library – Summary documentation, INDC(NDS)-0628, IAEA, Vienna (2012).

[24] Fusion Evaluated Nuclear Data Library Ver.3.1d, 2018
<https://www-nds.iaea.org/fendl31d/>